

## **Modifications of unpromoted and cobalt-promoted MoS<sub>2</sub> during thermal treatment by dimethylsulfide**

Gilles Berhault, Leonel Cota Araiza, Alberto Duarte Moller, Apurva Mehta, and Russell R. Chianelli.

Previous results have shown that the active surface in stabilized active sulfide catalysts is carbided. This fact led us to reconsider the influence of organosulfide agents in the activation of hydrotreatment catalysts. Structural and morphological consequences of dimethylsulfide treatment of (Co)/MoS<sub>2</sub>-based solids were studied. Results suggest that the electronic promotion of Mo by Co substantially influences the carbon replacement of sulfur atoms at the edges of molybdenum sulfide layers.

Key words: MoS<sub>2</sub>; MoS<sub>x</sub>C<sub>y</sub>; CoMoS; CoMoC; hidryodesulfurization; dimethylsulfide

### **Introduction**

Hydrotreating processes are used extensively in refineries to improve the environmental quality of liquid transportation fuels. Elevated temperatures (573–673 K) and high hydrogen pressures are required in this catalytic process to carry out hydrogenolysis reactions of C–S, C–N, C–O or C–metal bonds [1]. Catalysts used to perform these reactions are sulfide catalysts, particularly molybdenum or tungsten sulfides supported on alumina and promoted by cobalt or nickel. Since the seventies, many studies were made in order to understand the nature of the Co or Ni synergetic effect on molybdenum sulfide. The first detailed model describing electronic promotion was proposed by Voorhoeve and Stuiver [2] and Farragher and Cossee [3]. In this model, the promotion effect was the result of a charge transfer from pseudo-intercalated

Ni promoting atoms to  $W^{4+}$  creating  $W^{3+}$  sites. The first evidence of a particular Co environment was demonstrated through studies performed by Topsøe *et al.* [4]. They showed the existence of the so-called “CoMoS” phase in which Co atoms were located at the edges of  $MoS_2$  crystallites in a “decoration” mode. The existence of the “CoMoS” as a “precursor” phase is well established. However, recent results have shown that, in real hydrotreating conditions (triphasic reactor with a liquid phase made of a complex mixture of hydrocarbons leading to a very high partial pressure of “carbon” compounds), the stabilized active phase contains structurally important amounts of carbon which up to this point has been largely ignored [5]. Early evidence of a carbidic nature of the active phase was found in the patents of Chianelli and Pecoraro [6, 7] and of Seiver and Chianelli [8]. More recent studies have confirmed this initial observation showing that the final stoichiometry of the active phase should be viewed as  $MoS_yC_z$  with carbon replacing some sulfur atoms on the edges of the molybdenum sulfide hexagonal lattice.

This final “carbosulfide” surface state can be obtained through different methods. Firstly, this stabilized phase was prepared after catalyzing the desulfurization of dibenzothiophene in a decalin carrier with usual hydrotreatment conditions (350 °C, 35 atm  $H_2$ ) using a Carberry reactor [5]. This  $MoS_yC_z$  stoichiometry could also be obtained through the decomposition of a tetraalkylthiomethylate precursor, i.e.,  $(NR_4)_2MeS_4$  (Me = Mo, W) [9,10]. Finally, in a previous study, Berhault *et al.* [11] have shown that the interaction of dimethylsulfide (DMS) with an unsupported molybdenum sulfide catalyst could equally achieve a  $MoS_yC_z$  final stoichiometry. Using bulk and surface techniques and molecular simulations as well, they were able to characterize the structural and morphological consequences of the DMS– $MoS_2$  interaction. While the bulk phase stays

sulfidic by nature, the surface presents a carbidic character with carbon replacing surface sulfur atoms. The initial  $\text{MoS}_{2+x}$  stoichiometry gives rise to a final  $\text{MoS}_y\text{C}_z$  phase with  $y+z=2+x$  in the presence of a hydrogen atmosphere while excess carbon is present if the DMS treatment is performed under a nitrogen atmosphere. Apart from this structural modification, morphological consequences are also observed with the formation of better dispersed crystallites after the DMS treatment particularly when a nitrogen atmosphere is used. These results led us to reconsider the role of carbon in hydrotreating applications, mainly the activation of sulfide catalysts by organosulfide agents (dimethylsulfide, dimethyldisulfide, alkylpolysulfides, etc.). Indeed, it is well known that activation by carbon-containing sulfiding agents enhances the hydrodesulfurization (HDS) activity [12–14]. It should also be mentioned that, if one starts with a bulk carbide catalyst, the active phase in the presence of sulfur reactants tends to a carbosulfide surface phase similar to the one observed in sulfide catalysts [15, 16]. The objective of this work is to give an overview of the structural modifications of both unpromoted and cobaltpromoted  $\text{MoS}_2$  phases with particular attention to the influence of the promotion over the degree of carburization of the initial  $\text{MoS}_2$  system. A tentative model is presented in order to explain the C–S exchange on the surface of  $\text{MoS}_2$  catalysts and the morphological consequences inherent to this carbon inclusion.

## **Experimental**

### *Catalyst preparation*

#### *Synthesis of the $(\text{NH}_4)_2\text{MoS}_4$ and Co/ $(\text{NH}_4)_2\text{MoS}_4$ precursors*

The  $(\text{NH}_4)_2\text{MoS}_4$  precursor was readily prepared by adding  $(\text{NH}_4)_2\text{S}$ , 42.5% in aqueous solution to  $(\text{NH}_4)_6[\text{Mo}_7\text{O}_{24}]\cdot 4\text{H}_2\text{O}$  diluted in a minimal amount of water. This

preparation has been described previously [11]. For the cobalt-containing precursor,  $\text{CoCl}_2 \cdot 6\text{H}_2\text{O}$  was added to the red orange solution of  $(\text{NH}_4)_2\text{MoS}_4$  in the atomic proportion,  $\text{Co}/(\text{Co} + \text{Mo}) = 0.3$ . Immediately, a black precipitate is formed. The precipitate was washed several times with isopropanol before drying on a vacuum filter.

#### *Thermal decomposition of $\text{Co}/(\text{NH}_4)_2\text{MoS}_4$ into $\text{Co}/\text{MoS}_{2+x}$*

The precursor was thermally decomposed under  $\text{N}_2$  at given temperature for 2 h (heating rate  $2.5 \text{ Kmin}^{-1}$ ,  $\text{N}_2$  flow  $60 \text{ cm}^3 \text{ min}^{-1}$ ). The temperature of the thermal treatment was modified to vary the S/Mo ratio. At temperatures higher than 573 K,  $\text{MoS}_{2+x}$  was obtained through decomposition of  $\text{MoS}_3$  (the value of x decreases with increasing temperature until pure  $\text{MoS}_2$  is obtained). After this treatment, the solids were cooled down to room temperature (RT) under  $\text{N}_2$  and stored in sealed bottles.  $\text{MoS}_2$  and  $\text{Co}/\text{MoS}_2$  samples were labeled MST or CMST with  $T$ , temperature of  $\text{N}_2$  treatment in K.

#### *Dimethylsulfide thermal treatment*

$\text{MoS}_2$  samples (100 mg) were flushed under  $\text{N}_2$  at RT for 15 min before being contacted with a mixture of  $\text{CH}_3\text{--S--CH}_3$  (DMS) diluted in  $\text{N}_2$  or  $\text{H}_2$ . The DMS partial pressure was fixed at 180 Torr (24.0 kPa). The solids were then heated under this flowing reactant mixture up to a given temperature ( $573 \text{ K} < T < 833 \text{ K}$ ) at a heating rate of  $2.5 \text{ Kmin}^{-1}$  and maintained at this temperature for 1 h. The samples were then cooled to RT in the presence of the  $\text{N}_2$  ( $\text{H}_2$ )/ $\text{CH}_3\text{--S--CH}_3$  mixture, flushed for 2 h with  $\text{N}_2$  and stored in sealed bottles under Ar. Elemental analyses (Mo, S and C contents) were performed by Galbraith Laboratories, Inc. Sulfur content overestimation was corrected

using a crystalline MoS<sub>2</sub> sample (MoS<sub>2</sub> single crystal from Climax Molybdenum, Inc.) as a reference.

### *FTIR spectroscopy*

The samples were characterized by infrared spectroscopy in the 4000–200 cm<sup>-1</sup> wavenumber range. Samples were prepared by dilution in CsI powder (WilmaD, Infrared Grade) in a 1% mass ratio. CsI powder was preferred due to its high transparency in the far-infrared region until 180 cm<sup>-1</sup>. The IR spectra were recorded using an ATI Mattson Infinity 60 AR spectrometer. The far-infrared domain (<500 cm<sup>-1</sup>) as well as the mid-IR region was inspected with a DTGS detector equipped with a PE window (far-IR) and a CsI beamsplitter. Spectra were then recorded in the 2000–180 cm<sup>-1</sup> region, for higher wavenumber domains, acquisitions were carried out by switching to a KBr beamsplitter. Band intensities were corrected for slight differences in weight. Spectra treatment was carried out using the IR Winfirst software. FTIR spectroscopy was used either to characterize MoS<sub>2</sub> samples treated in a flow reactor in the presence of CH<sub>3</sub>–S–CH<sub>3</sub> or to prepare directly in situ carbided MoS<sub>2</sub> samples. This alternative preparation was made by heating a 1% MoS<sub>2</sub>/CsI pellet in the presence of 10 Torr of DMS. The KBr window-equipped cell was previously evacuated at RT before contact with DMS. The pellet was then heated to a given temperature at 2.0 Kmin<sup>-1</sup> and maintained at this temperature for 1 h. The sample was then cooled down until RT in the presence of CH<sub>3</sub>–S–CH<sub>3</sub> and then evacuated for 2 h. Spectra were then recorded without any contact with air.

### *Synchrotron XRD*

Synchrotron XRD experiments were performed at the Stanford Synchrotron Radiation Laboratory on beamline 2-1. The high brightness and vertical collimation of the

synchrotron beam allow use of a Si(111)-based detector able to resolve lattice parameter changes of the order of 0.1%. The size of the focused beam is  $2 \times 1$  mm and approximately  $10^{11}$  photons/s are incident on the sample at an energy of  $1.0 \times 10^4$  eV ( $\lambda = 1.2389$  Å). The XRD patterns were collected in the  $4^\circ$ – $104^\circ$   $2\theta$  range with an increment of  $0.1^\circ$ . The synchrotron source was used to determine structural differences before and after the carbiding process under a nitrogen atmosphere. A higher temperature of treatment (833 K) than normally present in hydrotreating conditions is used in order to emphasize the interaction of the DMS treatment with the molybdenum disulfide phase.

#### *Electron energy loss spectroscopy*

The samples were ultrasonically dispersed in ethanol. A drop of the suspension was then placed in a holey carbon Cu grid. The observations were performed with a Jeol 2010 transmission electronmicroscope equipped with a Gatan 666 parallel spectrometer. Attention was devoted to the vicinity of the C K-edge transition region around 300 eV.

#### *Molecular simulations*

The Crystal Builder, Surface Builder, Interface Builder, Force-Field, IR/Raman, Diffraction Crystal and Rietveld (DBWS) modules of the Cerius<sup>2</sup> 4.0 simulation package of Molecular Simulation Inc. (MSI) were used to compare experimental XRD and IR results with a theoretical model of the structure and stability of bulk MoS<sub>2</sub>. The crystalline models were generated using the Crystal Builder module (MoS<sub>2</sub> atomic positions, symmetry conditions and lattice parameters). The minimum energy

configuration was calculated using a force–fieldWestheimer method based on the Born–Openheimer approximation.

## Results

Unsupported  $\text{MoS}_2$  catalysts were prepared by decomposition of ATTMM (ammonium tetrathiomolybdate,  $(\text{NH}_4)_2\text{MoS}_4$ ) under an inert gas. The thermal decomposition of ATTMM was chosen for preparation of samples because this method provides a simple and reproducible method for preparing pure  $\text{MoS}_2$  catalysts. Careful heating of the ATTMM precursor at increasing temperatures in a  $\text{N}_2$  atmosphere produces  $\text{MoS}_{2+x}$  bulk solids with  $x$  representing excess sulfur in the catalyst presumably located at the edges [5]. Figure 1 reports the variation of the overstoichiometric S/Mo ratio (called  $x$ ) with increasing temperature of treatment. Large S/Mo variations can be obtained using this procedure with  $x$  varying from 0.0 to 0.5. Stoichiometric  $\text{MoS}_2$  is progressively obtained as the excess sulfur and the edge area are vanishing.

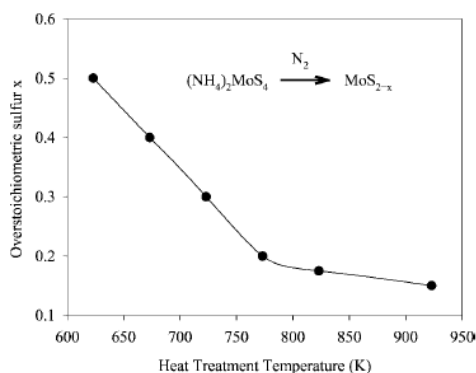


Figure 1. Variation of the overstoichiometric S/Mo ratio  $x$  of a typical  $\text{MoS}_{2+x}$  sample prepared from  $(\text{NH}_4)_2\text{MoS}_4$  (ATTMM) precursor in the presence of a  $\text{N}_2$  mixture.

The thermal decomposition of the  $(\text{NH}_4)_2\text{MoS}_4$  precursor was carefully followed in order to accurately evaluate the morphological changes due to the DMS treatment described later in this report.

*Infrared spectroscopy*

Figure 2 reports the evolution of the IR bands in the range 600–200  $\text{cm}^{-1}$  for different temperatures of treatment under  $\text{N}_2$ . The  $\text{MoS}_2$  sample obtained by ATTM thermal decomposition at 573 K (MS573) presents very weak bands at 385, 468 and 530  $\text{cm}^{-1}$ . Increasing the temperature about 30 K causes an increase of the 385 and 467  $\text{cm}^{-1}$  band while the 530  $\text{cm}^{-1}$  signal stays relatively constant. The 385 and 467  $\text{cm}^{-1}$  signals are assigned to the Mo–S stretching modes of vibrations, respectively, along the basal plane ( $E \perp c$ , 385  $\text{cm}^{-1}$ ) and perpendicularly to the basal plane ( $E \parallel c$  467  $\text{cm}^{-1}$ ) [17]. Treatment at higher temperatures ( $T > 773$  K) is associated with increasing and sharpening of the two  $\nu(\text{Mo-S})$  modes while the 530  $\text{cm}^{-1}$  broad band progressively vanishes. This signal is ascribed to  $(\text{S-S})^{2-}$  bands coming from the linking of small  $\text{MoS}_2$  slabs, which are located at the edges [18]. For cobalt-promoted  $\text{MoS}_2$  phase, spectra were oversimplified and the Mo–S stretching bands generally appeared very weak, as observed by Schrader and Cheng [19]. The absence of a broad profile centered on 330  $\text{cm}^{-1}$  even at 573 K suggests that the amorphous  $\text{MoS}_3$  phase has already been decomposed at this temperature and the  $\text{MoS}_2$  local structure is emerging [20]. Moreover, the increase of temperature enhances more strongly the 385  $\text{cm}^{-1}$  intensity peak than the 467  $\text{cm}^{-1}$  one. This effect could be related to a more rapid increase of the stacking number of the  $\text{MoS}_2$  layered structure compared to the particle growth along the basal plane.



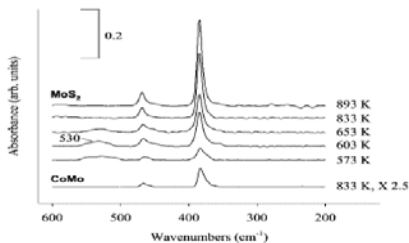


Figure 2. Far-IR spectra ( $600\text{--}200\text{ cm}^{-1}$ ) of unsupported  $\text{MoS}_2$  samples prepared by ATTM thermal decomposition under  $\text{N}_2$  at different temperatures of treatment (upper part) and of  $\text{Co-MoS}_2$  prepared in the same conditions at 833 K (lower part). Conditions: heating rate  $2.5\text{ K min}^{-1}$ , 2 h at temperature  $T$ ,  $\text{N}_2$  flow  $60\text{ cm}^3/\text{min}$ .

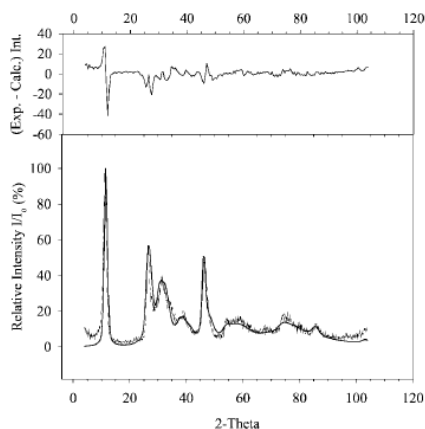


Figure 3. Comparison between experimental and simulated synchrotron XRD patterns of an MS833 sample ( $\text{MoS}_2$  prepared from ATTM under  $\text{N}_2$  at 833 K, 2 h). The upper graph represents the difference between these two patterns.

### Synchrotron X-ray diffraction

Further insight regarding the structure of  $\text{MoS}_2$  poorly crystalline samples was obtained using the SSRL (Stanford Synchrotron Radiation Laboratory) X-ray source. The powder diffractometer operating with an intense monochromatic beam ( $\lambda = 1.2389\text{ \AA}$ ) was used to record the XRD pattern of an MS833 ( $\text{MoS}_2$  833 K ATTM decomposition in  $\text{N}_2$ ) sample. The higher resolution and superior signal to noise of this technique was readily apparent. As reported in figures 3 and 4,  $\text{MoS}_2$  and  $\text{Co/MoS}_2$  diffractograms are typical of a poorly crystalline  $\text{MoS}_2$  phase [21] with the most intense peak at  $2\theta = 11.2^\circ$  ( $\lambda = 1.2389\text{ \AA}$ ) and a broad envelope beginning approximately at  $25^\circ$  and continuing above  $2\theta = 45^\circ$  and characterized by the asymmetric shape of the (100) diffraction peak at  $2\theta = 26.5^\circ$ . This experimental pattern was fitted to a simulated pattern using the

Crystal Diffraction and Crystal Builder modules from Cerius2 4.0 (Molecular Simulations Inc.). Figure 3 reports the fitting results between experimental and simulated patterns as well as the difference of the two spectra (upper part). Quite satisfactory fitting was obtained using the 3R-MoS<sub>2</sub> crystallographic structure instead of a 2H-MoS<sub>2</sub> structure (space group: R3m unit cell dimensions:  $a = 3.16 \text{ \AA}$ ,  $c = 18.42 \text{ \AA}$ ). At low angles, the background presents a relatively high non-Bragg scattering. This is due to a highly disordered structure (“rag structure”) in which individual MoS<sub>2</sub> layers are randomly folded and connected to each other. Additionally, the difference in the experimental and the calculated pattern for the (002) peak was attributed to preferential orientation. Moreover, on standard XRD patterns, it should be noted that the low-angle non-Bragg scattering signal disappears after a treatment at 893 K (not shown here) compared with the 833 K treatment.

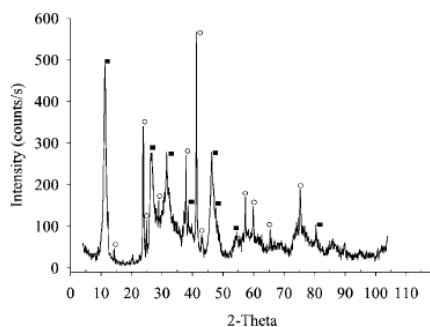


Figure 4. Synchrotron XRD pattern of a CMS833 sample (treatment under N<sub>2</sub> at 833 K, 2 h from Co/ATM precursor). (■) MoS<sub>2</sub>, (○) Co<sub>9</sub>S<sub>8</sub>.

This shows that the disorder due to randomly folded layers is reduced. Meanwhile, the asymmetric shape of the (100) peak at  $2\Theta = 34^\circ$  peak still remains, indicating the presence of turbostratic MoS<sub>2</sub> (random layer lattice) which is typical of molybdenum-sulfidebased catalysts. A Rietveld refinement study confirmed the assignment of our starting material to a 3R structure. Starting from a 50% 3R–50% 2H mixed contribution in the experimental pattern, the best refinement gave a 94% 3R–6%

2H result. This 3R assignment was already observed starting from  $(\text{NH}_4)_2\text{MoS}_4$  [22]. To distinguish between the 3R (rhombohedral) and 2H (hexagonal)- $\text{MoS}_2$  structures is quite difficult with standard XRD techniques and the quality of the synchrotron source is thus strikingly seen. Indeed, the two crystallographic structures are differing only in the layer sequence. In the 2H stacking sequence, compared to the first layer, the second layer is slightly shifted along the  $a$  axis from the first layer while the third one will be in the same atomic position. In the 3R sequence, only the fourth layer will be in the same atomic positions as the first one. From a catalytic point of view, the consequence of this slight difference is unknown. According to the “rim-edge” model [23], this different layer arrangement could probably induce some changes in selectivity.

Figure 4 reports the synchrotron XRD pattern of the CoMo sample after  $\text{N}_2$  treatment at 833 K (CMS833). Apart from the diffraction peak characteristic of a poorly crystalline  $\text{MoS}_2$  phase, quite intense peaks corresponding to  $\text{Co}_9\text{S}_8$  are observed at  $23.8^\circ$  (311),  $37.8^\circ$  (333),  $41.3^\circ$  (440),  $57.3^\circ$  (731) + (553),  $59.9^\circ$  (800) and  $75.3^\circ$  (844). As expected from the lesser stability of the promoted catalysts, the high temperature of treatment (833 K) is responsible for the segregation of the Co/ $\text{MoS}_2$  catalyst into their respective monosulfide phases, *i.e.*,  $\text{MoS}_2$  and  $\text{Co}_9\text{S}_8$  [24].

#### *Thermal treatment with dimethyl sulfide*

A real industrial hydrotreating unit is a triphasic reactor with a solid catalyst, hydrogen gas and a liquid phase composed of a complex mixture of hydrocarbons. Hydrogen must diffuse from the gas phase to the liquid one, solubilize, and then diffuse from the liquid phase to the catalyst surface before undergoing a dissociative chemisorption step, a prerequisite to the C heteroelement hydrogenolysis [25].

Therefore, two different dimethylsulfide treatments using nitrogen or hydrogen atmosphere were used in order to clarify the interaction of H<sub>2</sub> (or N<sub>2</sub>) with DMS during the thermal treatment.

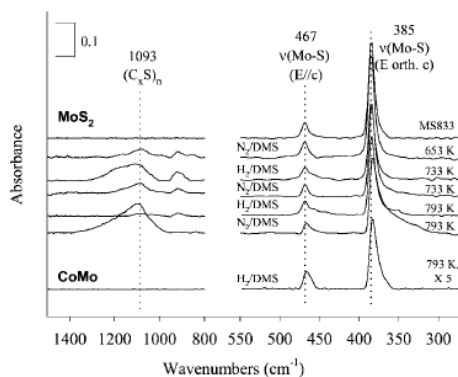


Figure 5. Evolution of the IR spectra of cobalt-promoted (lower part) and unsupported MoS<sub>2</sub> (upper part) samples recorded at different temperatures of DMS treatment under a N<sub>2</sub> (or H<sub>2</sub>) atmosphere in the mid-IR wavenumber region (1400–800 cm<sup>-1</sup>) and in the far-IR region (550–300 cm<sup>-1</sup>).

#### *Infrared characterization after treatment under a DMS flow (dynamic mode)*

Figure 5 reports the evolution of IR spectra recorded at different temperatures of DMS treatment under N<sub>2</sub> or H<sub>2</sub> atmospheres. A decrease of the intensity of the 385 cm<sup>-1</sup> signal is observed as the temperature of treatment is increased. Moreover, the two Mo–S stretching bands gradually exhibit an asymmetric shape at lower wavenumbers. In the mid-IR region, intermediary products of the DMS decomposition as (C<sub>x</sub>S)<sub>n</sub> polymer species are characterized by a broad band at 1093 cm<sup>-1</sup> as well as a minor signal at 830 cm<sup>-1</sup> [26]. As the N<sub>2</sub> temperature increases, these peaks are more intense indicating a further production of polymeric species. Using hydrogen at high temperature removes these (C<sub>x</sub>S)<sub>n</sub> moieties for both unpromoted and cobalt-promoted samples.

#### *Infrared characterization by direct in situ CH<sub>3</sub>–S–CH<sub>3</sub> decomposition (static mode)*

A 100 mg CsI pellet with 1 w% of MoS<sub>2</sub> was heated at 2 Kmin<sup>-1</sup> in the presence of 10 Torr of CH<sub>3</sub>-S-CH<sub>3</sub> up to a given temperature *T* and maintained 1 h at this temperature. The sample was then cooled down to RT before evacuation at moderate vacuum in a first step (10<sup>-3</sup> Torr) before a complete evacuation at 10<sup>-6</sup> Torr 2 h. Spectra were recorded without any contact with air and the mid-IR region was investigated.

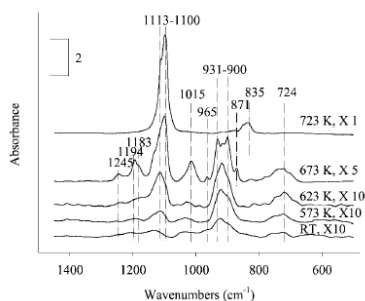


Figure 6 presents the spectra in the 1450–600 cm<sup>-1</sup> wavenumber region for an MS773 sample (MoS<sub>2</sub> 773 K ATTM decomposition in N<sub>2</sub>). The C–S–C “skeleton” gives rise to absorption bands due to the  $\nu(\text{CSC})$  stretching modes between 780 and 690 cm<sup>-1</sup> [27,28]. The methyl groups exhibit rocking modes of vibration at 1015, 965 and between 930 and 870 cm<sup>-1</sup>.  $\delta(\text{CH}_3)$  bending modes at 1464, 1408 and 1345 cm<sup>-1</sup> as well as the  $\nu(\text{CH}_3)$  stretching bands at 2915 and 2986 cm<sup>-1</sup> are very weak. Harmonic bands combining rocking modes and bending modes of the C–S–C skeleton are detectable at 1245, 1194 and 1182 cm<sup>-1</sup>. A strong peak is also observed around 1100 cm<sup>-1</sup> with a shoulder at 1113 cm<sup>-1</sup> and is assigned to a  $\nu(\text{C}=\text{S})$  vibration [26]. The intensity of the peaks due to the CH<sub>3</sub>-S-CH<sub>3</sub> adsorption increases as far as a temperature of treatment of 673 K. The 723 K treatment involves the disappearance of any peaks due to a CH<sub>3</sub>-S-CH<sub>3</sub> adsorption, only the high intense  $\nu(\text{C}=\text{S})$  band is still present with a minor contribution at 835 cm<sup>-1</sup>. The gas phase spectrum clearly showed the formation of methane. All the vibrations due to the CSC skeleton or due to methyl groups have

completely vanished. These results showed that, in the absence of H<sub>2</sub>, CH<sub>3</sub>-S-CH<sub>3</sub> adsorbed irreversibly on the MoS<sub>2</sub> surface up to 673 K while, between 673 and 723 K, the DMS species decompose and only the formation of “carbosulfide” polymer species is detectable.

### *Electron energy loss spectroscopy (EELS)*

EELS spectra records the scattered intensity of an electron beam passing through a target compound as a function of the decrease in kinetic energy. Repulsion from inner or outer shell atomic electrons of the analyzed sample provokes an inelastic scattering for the transmitted electrons at highenergy loss and low-energy loss values, respectively. For inner-shell excitation, scattering is characterized by edges whose energy-loss values correspond to the binding energy of the atomic shell under consideration.

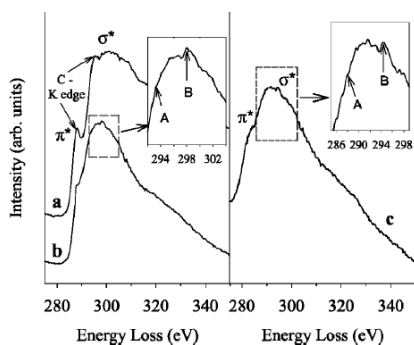


Figure 7. EELS C K-edge shapes (280–340 eV) of (a) a  $\beta$ -Mo<sub>2</sub>C reference, (b) an MS833 sample treated at 793 K with N<sub>2</sub>/DMS at a DMS partial pressure of 180 Torr (24.0 kPa) and (c) a CMS833 sample treated in the same conditions as (b). The inset presents the fine structure shape observed at the  $\sigma^*$  transition.

The intensity of this “ionization threshold” is related to a particular element. These ionization edges possess a fine structure reflecting the energy-band structure of the studied element. Thus, EELS C K-edge shapes can help in differentiating between various carbon structures. Figure 7 reports the EELS C K-edge spectra for a  $\beta$ -Mo<sub>2</sub>C reference and for the MS833 and CMS833 samples, both treated at 793 K with DMS

(180 Torr) diluted in N<sub>2</sub>. Two transitions corresponding to the  $\pi^*$  and  $\sigma^*$  antibonding states can be observed. As reported previously [11], for amorphous carbon, the C K-edge presents a smooth shape without noticeable peaks for the  $\pi^*$  and  $\sigma^*$  states. For graphite and carbide, two features A and B are detectable in the  $\sigma^*$  region. Their relative intensities correspond to a different density of states [29]. In the graphitic structure, carbon sp<sup>2</sup> bonds imply that A is at higher intensity than B whereas, for a carbidic structure, carbon sp<sup>3</sup> bonds are related to a higher intensity of feature B compared to A. Analysis of the fine structure of both MS833 and CMS833 samples confirm that B is at higher intensity than A. Consequently, the carbon structure does not appear graphitic. The surface structure reveals the presence of Mo–C bonds of a carbide-like structure. However, the  $\pi^*$  shape is smoother than for pure Mo<sub>2</sub>C revealing that a part of the carbon is also of amorphous nature. The presence of amorphous carbon and the absence of an organized graphitic structure was checked previously by high-resolution electron microscopy (HREM) and near-edge X-ray absorption fine structure (NEXAFS) spectroscopy [11]. NEXAFS also undoubtedly revealed the formation of a carbide-like structure on the MoS<sub>2</sub> surface [11].

EELS results confirm the formation of metal–carbon bonds at the surface of unsupported MoS<sub>2</sub> and Co/MoS<sub>2</sub> catalysts after DMS treatment. Moreover, careful study of the C K-edge fine structure reveals that features A and B are shifted 6 eV downwards for the DMS-treated Co/MoS<sub>2</sub> samples compared to MoS<sub>2</sub>. This suggests strongly a weakening of the Me–C bond strength in the DMS-treated CoMo sample, which could be related to the electronic donation from Co to carbon-coordinated Mo.

*Synchrotron X-ray diffraction*

Synchrotron XRD studies were performed to check if the carbide-induced modification of the DMS-treated unsupported MoS<sub>2</sub> and Co/MoS<sub>2</sub> catalysts is restricted to the outermost layers or if carburization occurs deeply inside the bulk structure. As reported in figure 8 (lower part), for the unpromoted catalyst, the XRD pattern is typical of a MoS<sub>2</sub> layered structure. No new peaks are detected. However, careful analysis reveals that the intensity of the (110) plane at 2 $\Theta$ = 47° is surprisingly higher than this one for the (100) plane. Using the Crystal Builder and Crystal Diffraction modules from Cerius2 4.0 (Molecular Simulations Inc.), fitting calculations between experimental and simulated patterns showed that this more intense (110) peak could be ascribed to a higher distortion (more folding) of the layered structure along the c axis following the DMS treatment. A quite different pattern was observed for the cobalt-promoted MoS<sub>2</sub> catalyst (upper part, figure 8). As already observed in figure 4, treatment at 833 K involves a phase segregation of the MoS<sub>2</sub> and Co<sub>9</sub>S<sub>8</sub> phases. However, diffraction peaks of the Co<sub>9</sub>S<sub>8</sub> phase are less intense than on the non-DMS treated CoMo catalyst.

This suggests that crystallization of the cobalt sulfide phase is slightly retarded by the DMS treatment. This could be related to a retardation effect of amorphous carbon on the crystallization of sulfide phases [30, 31]. Moreover, even if the intensity of the (110) plane remains important, the ratio  $I(110)/I(100)$  somewhat decreases suggesting a slightly less bending effect on the remaining MoS<sub>2</sub> phase. More interestingly, new diffraction peaks corresponding to a Mo<sub>2</sub>C-like hexagonal phase appear. Indeed, molybdenum carbide peaks are observed at 2 $\Theta$  = 28.1° (100), 30.6° (002), 31.2° (101), 43.0° (102), 54.2° (103) and 58.4° (112)+(201). A diffraction peak corresponding to the (110) plane is expected at 2 $\Theta$  = 48.6° but is overlapped by the intense (110) diffraction



peak of the MoS<sub>2</sub> phase. This result demonstrates that cobalt promotion has a strong influence on the degree of carburization of the MoS<sub>2</sub> phase when contacting to an organosulfide agent.

## Discussion

In our previous studies [5,11], we have evidenced that carbon plays an important role in hydrotreatment modifying structurally the nature of the stabilized active phase in real hydrotreating conditions. This fact has pushed us to explore the consequences of the interaction of carbon-containing sulfiding agents with transition metal sulfides. Indeed, it is well known that organosulfide agents (CH<sub>3</sub>-S-CH<sub>3</sub>, CH<sub>3</sub>-S-S-CH<sub>3</sub>, alkylpolysulfides, etc.) improve activity of the final active phase [12]. Previous studies as well as the present one, through surface sensitive techniques, showed that the surface species present on MoS<sub>2</sub> and Co/MoS<sub>2</sub> catalysts are not only coordinately unsaturated sites (CUS), sulfhydryl (SH), S<sup>2-</sup> or 2  $\frac{2}{2}$ - entities but also carbonmoieties with a carbidic nature. However, the extent of this carburization effect is unknown at this point. Results obtained by Oyama and co-workers [15,16] demonstrated that the catalytic compartment of molybdenum carbide catalysts in hydrodesulfurization reactions tends to a final “carbosulfide” phase. It should be reasonably envisaged that the surface concentrations of the different species will reach an equilibrium between sulfur and carbon entities depending on reaction conditions. Otherwise, for similar conditions of treatment, we already obtained information for unsupported MoS<sub>2</sub> catalysts. IR molecular simulations were performed using the Force-Field and IR/Raman module of Cerius<sup>2</sup> 4.0 (MSI Inc.). These fitting simulations were based on direct approximate calculations and not on density functional techniques (DFT) even if former DFT studies

[32] were taken into account in order to first refine the MoS<sub>2</sub> crystallographic structure and secondly to build a definite 60 Å length model slab. Considering as observed by DFT only slight relaxation processes on the edges of MoS<sub>2</sub> slabs, our model fits well experimental Mo–S stretch frequencies at 385 and 467 cm<sup>-1</sup>. As for oxidation reactions, a “cherry” model was then assumed with carburization progressing from the edges to the bulk of the model slab. Results showed that the asymmetric tail observed on IR spectra of DMS-treated MoS<sub>2</sub> samples is partly a result of carbon replacement of surface sulfur atoms through a topotactic process and/or bending of the layers. This topotactic process was already observed by Lee *et al.* [33] in a study about the α-MoC<sub>1-x</sub> formation from MoO<sub>3</sub>. HREELS experiments have indicated that the Mo–C stretching mode of vibration gives rise to signals in the 360–380 cm<sup>-1</sup> wavenumber range [34]. However, no ν(Mo–C) signal was detectable in our β-Mo<sub>2</sub>C IR spectra due to the Mo–Mo metallic interaction of this compound. In the present case, the detection of a ν(Mo–C) signal would be due to the fact that the carbide phase is supported on a MoS<sub>2</sub> bulk structure, well known to possess semiconducting properties [35]. More interestingly, these results confirmed that for MoS<sub>2</sub>, the carburization replacement process is a surface reaction occurring only at the edges of MoS<sub>2</sub> slabs without progressing inside the bulk structure. A more advanced carburization effect will probably provoke phase segregation into MoS<sub>2</sub> and Mo<sub>2</sub>C and is unrealistic considering temperature ranges.

As already mentioned, Boudart and co-workers [33] showed that molybdenum carbide synthesis from MoO<sub>3</sub> can occur through a topotactic process in which the synthesized metastable α-MoC<sub>1-x</sub> phase exhibits pseudomorphism with the original

platelets of  $\text{MoO}_3$ . A similar process can be envisaged in the present case.

Morphological consequences of the formation of a carbosulfide phase could be approached through the formation of a mixed C–Mo–S sandwich layered structure. In a first step, the  $\text{Mo}_2\text{C}$  structure was built based on a hexagonal close-packed configuration of Mo layers with carbon in octahedral holes. A simulated XRD pattern was calculated and compared to literature data [36]. A quite good agreement is found with main peaks at  $34.5^\circ$ ,  $38.0^\circ$ ,  $39.6^\circ$ ,  $52.2^\circ$ ,  $61.9^\circ$  and  $75.9^\circ$  corresponding, respectively, to the (100), (002), (101), (102), (110) and (201) reflections. Next, an interface along the (001) planes of  $\text{Mo}_2\text{C}$  and  $\text{MoS}_2$  was constructed. Surface cleavage along the (001)  $\text{Mo}_2\text{C}$  and  $\text{MoS}_2$  planes exhibit a very similar configuration, as shown in figure 9. Indeed, angles and nonmetal–nonmetal distances are quite close with a C–C distance of  $3.00 \text{ \AA}$  and a S–S distance of  $3.16 \text{ \AA}$ .

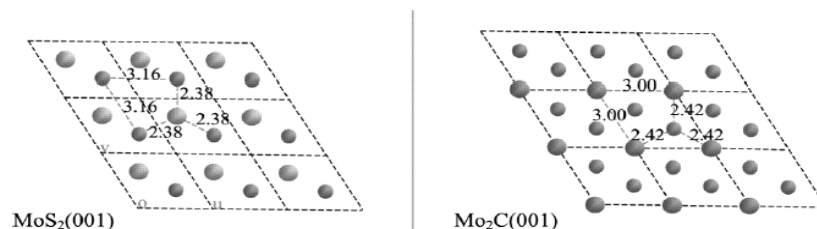


Figure 9. Comparison of the two (001) surface cleaved  $\text{MoS}_2$  and  $\beta\text{-Mo}_2\text{C}$ . C(S)–Mo and C(S)–C(S) distances are indicated. Left side: Mo (small circles), S (large circles); right side: Mo (small circles), C (large circles). Metal–metal and sulfur (resp. carbon)–metal distances are indicated in  $\text{\AA}$ .

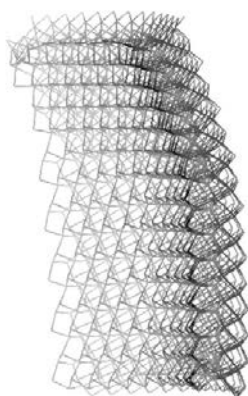


Figure 10. Example of a  $40 \text{ \AA} \times 40 \text{ \AA}$   $\text{MoS}_2(001)\text{-Mo}_2\text{C}(001)$  interface after energy minimization (1500 iterations). A strong bending effect is observed with convexity on the sulfur side.

The underlying Mo layer is at the center of a prism with a distance to the nearest nonmetal atoms of 2.42 and 2.39 Å, respectively, to carbon and sulfur. Therefore, the as-built interface along their respective (001) planes shows a good matching between C and S. The total energy of the Mo<sub>2</sub>C–MoS<sub>2</sub> interface was minimized in order to determine the morphological consequences of the formation of a mixed C–Mo–S sandwich. As reported in figure 10, a strong bending effect is observed. In this particular case of a 40 Å×40 Å interface, the bending angle reaches a value of 18°. This is in good agreement with previous results showing that MoS<sub>2</sub> nanotubes with lower diameter than 10 nm are energetically highly improbable due to strong strain forces on the Mo–S bond [37]. In this particular case, the curving radius would be 13 nm. As a matter of fact, fitting calculations on XRD results have also indicated a higher folding for DMS-treated MoS<sub>2</sub>. However, this simulation does not correspond to a real modification of the particle shape. A so asymmetrical carburization process progressing only along one of the two S layers of the S–Mo–S sandwich without any replacement on the other side seems difficult to envisage. Nevertheless, as observed through the experimental results, a cherry model is acceptable with only replacement of sulfur atoms by carbon along the first outermost rows of the particle whereas the bulk structure remains sulfidic by nature. This effect has also been observed when an H<sub>2</sub>/H<sub>2</sub>S activated MoS<sub>2</sub> exfoliates in high vacuum in the presence of residual carbon [5,38]. This high reactivity of the MoS<sub>2</sub> edges versus carbon was also observed in previous results [39] and calculations on bent MoS<sub>2</sub> particles have recently been investigated [37]. bent extremities suggest that the carbon replacement process occurs only along the MoS<sub>2</sub> edges and does not interfere with inner Mo rows. The bending consequence of the formation of this C–Mo–S

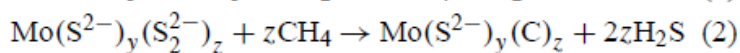
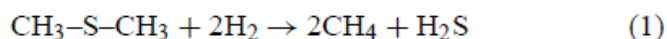
sandwich would be related to a slightly smaller Mo–S distance compared to the Mo–C one; indeed, the bending curve appears convex on the sulfur side. Thus, a part of the asymmetric shape observed for the IR peaks corresponding to Mo–S stretching modes could be due to this folding effect. This experimental curved shape of the MoS<sub>2</sub> edges would signify that the C replacement process does not progress so symmetrically on each side of the S–Mo–S trilayer with probably a more advanced carburized effect on the “rim sites” [23] situated at the extremities of the stacked MoS<sub>2</sub> layers. However, the bending morphological consequences of the carbon inclusion could participate in a certain extent in the formation of less stacked and smaller crystallites after DMS treatment through exfoliation as already observed in some regions of electron micrographs. Indeed, as reported before [11], the DMS interaction could reduce by a factor of two stacking and particle size.

For cobalt-promoted MoS<sub>2</sub> catalyst, EELS, IR and XRD results confirm a carburization effect similar to this one observed for non-promoted MoS<sub>2</sub>. However, XRD results suggest that cobalt promotion involves a higher tendency to carburize. This could be related to the higher reducibility of CoMo compared to MoS<sub>2</sub>. Indeed, temperature programmed reduction (TPR) results have shown that cobaltpromoted MoS<sub>2</sub> phase can be reduced more easily than the unpromoted phase for temperatures higher than 650 K [40]. This property was ascribed to the well-known electronic origin of promotion since in the CoMoS phase, Co donates electron to Mo weakening the Mo–S bond strength. In this way, cobalt promotion will favor indirectly carburization through electronic donation, resulting in higher reducibility of the Mo–S moieties. However, it is worth mentioning that at temperatures commonly used in hydrotreating reactions (623

K), both cobalt-promoted and unpromoted MoS<sub>2</sub> phases present similar degrees of reduction [40,41]. This supports that for this temperature range the carbide-like molybdenum phase is still engaged into a CoMo entity. Reducibility would simply help in carburizing molybdenum and will favor a more carbidic nature of Mo when involved into a Co–Mo electronic interaction. Consequently, the CoMoS phase initially present could be considered as a precursor phase leading under hydrotreating conditions to a CoMoC entity for which Co favors the carburization process. However, the case described here is a limiting case. In the hydrotreatment process, many experimental parameters (nature of hydrocarbons, temperature or pressure of treatment, partial pressure of the different reactants) could influence the surface state. It appears reasonable to say that the surface could vary from a partly to a completed carbided nature.

If reducibility appears a key parameter in the carburization process, one basic question arises: which mechanism is involved in this reaction? IR results suggest a possible explanation. First of all, as observed in figure 5, if H<sub>2</sub> is not used or is insufficiently present, polymer species are formed by degradation of (CH<sub>3</sub>)<sub>2</sub>S species, probably initially coordinately bonded to the MoS<sub>2</sub> surface, as observed by Ziolk et al. [28]. These (C<sub>x</sub>S)<sub>n</sub> entities are probably a “dead-end” product, which partly hampers the carburization process. Oppositely, as observed in the gas phase, in the presence of hydrogen, methane is one of the main products of the CH<sub>3</sub>–S–CH<sub>3</sub> decomposition. Produced from (CH<sub>3</sub>)<sub>2</sub>S species already linked to the surface, this nascent CH<sub>4</sub> could interact efficiently with surface species. As a matter of fact, the H<sub>2</sub>/CH<sub>4</sub> reactant mixture is commonly used for reducing and carburizing MoO<sub>3</sub> precursor [42].

As shown in table 1, in the case of the unpromoted phase, similar final stoichiometries are obtained either starting from the thiosalt precursor,  $(\text{NH}_4)_2\text{MoS}_4$  ( $\text{Mo}^{\text{VI}}$ ) or from  $\text{MoS}_{2+x}$  (mainly  $\text{Mo}^{\text{IV}}$ ). Even if the final temperatures of DMS treatment differs by 40 K, only few modifications could be expected between the two stoichiometries of the carburized samples due to this parameter alone. However, even taking into account this, the amount of structural carbon seems equivalent whatever the initial oxidation state of molybdenum. Even if we cannot rule out a possible role of hydrocarbons produced from DMS in the reduction of Mo, this would not be a crucial point in achieving the final active phase; bulk  $\text{MoS}_2$  is thermodynamically more stable than bulk  $\text{Mo}_2\text{C}$ . On the other hand, previous results [5] have shown that a correlation exists between the overstoichiometric sulfur amount present in the initial state (cf. figure 1) and the final amount of structural carbon in the stabilized active phase. Even if the nature of the overstoichiometric sulfur is still in debate [43,44], studies suggest that these species would be terminal  $\text{S}_2^{2-}$  groups [45–47]. Moreover, while a quite distinct  $\nu(\text{S-S})$  signal was detected on  $\text{MoS}_{2+x}$  samples up to 673 K (cf. figure 2), after DMS treatment in this temperature range, we did not observe  $(\text{S-S})_2^-$  groups anymore. This would suggest a possible redox interaction between terminal  $\text{S}_2^{2-}$  groups on the edges of  $\text{MoS}_2$  layers and the nascent  $\text{CH}_4$  produced from the decomposition of coordinately bonded DMS, preferentially in the presence of hydrogen. A tentative mechanism could then be envisaged according to the following equations:



However, further studies are needed to sustain this proposed mechanism, mainly by determining decomposition products of the DMS–(Co)MoS<sub>2</sub> reaction. Moreover, if carburization proceeds more easily for cobalt-promoted system, the nature of the sulfur species replaced by carbon (S atoms linked only to Mo or S shared between Mo and Co) is still in question. It should also be noted that kinetics of decomposition will play an important role in attaining appropriate final active phase [6–8].

## Conclusions

The anisotropic nature of the layered molybdenum sulfide structure confers quite different site reactivity as a function of sulfur unsaturation degree. While basal planes with completely saturated sulfur atoms are catalytically inert, edge sites are now well known to be the only potential sites for hydrotreating reactions. Furthermore, it has recently appeared that the stabilized active phase in real hydrotreatment conditions actually presents a surface carbidic-like nature which lead us to reconsider the role of carbon. In this respect, organosulfide agents are known to be beneficial for achieving better hydrodesulfurization activity. Consequently, the interaction of carbon with transition metal sulfides was reinvestigated through the potential influence of organosulfur compounds in the activation process of catalysts.

Results showed that dimethylsulfide interacts with unpromoted MoS<sub>2</sub> through a carbon replacement of sulfur atoms located at the edges of the layers while the inherent low reactivity of saturated sulfur atoms limits this process to a surface chemistry type reaction. Cobalt promotion induces a higher tendency of the molybdenum sulfide phase to “surface carburization”. A possible link between reducibility of a given sulfide phase and its propensity to carbon replacement could thus be envisaged. For cobalt-promoted



systems, the higher degree of carburization might be related to a higher reducibility of Mo atoms involved in the initial CoMoS phase resulting from the electronic promotion from cobalt. Finally, both using a hydrogen or nitrogen atmosphere with DMS led to the formation of surface carbidic species even if this process of formation would probably be favored by the presence of hydrogen.

Apart from structural considerations, morphological consequences of the DMS–MoS<sub>2</sub> based solids interaction were observed. Previous studies have shown that the DMS treatment, particularly in the presence of a nitrogen atmosphere, leads to better dispersed MoS<sub>2</sub> particles with smaller and less stacked crystallites dispersed on “fluffy” amorphous carbon. This amorphous carbon involves a retardation effect on the crystalline growth stabilizing the active phase. Molecular simulations, IR and XRD results suggest that carbon inclusion into the MoS<sub>2</sub> structure could also induce a higher folding nature of the layers particularly at the edges (or in plane defects) and favor exfoliation process. Finally, based on the proportionality observed between the overstoichiometric sulfur content in the initial sulfide phase and the final amount of structural carbon, a tentative mechanism was proposed based on an interaction of hydrocarbons produced from DMS and terminal (S–S)<sub>2</sub><sup>2</sup> groups.

## **Acknowledgment**

This work was supported by a grant from the Government Services Administration, the US Department of Energy “Gateway” Program, the Robert A. Welch Foundation, the National Science Foundation, ATOFINA and the General Electric Faculty for the Future Program.

## **References**

- [1] B.C. Gates, J.R. Katzer and G.C.A Schuit, Chemistry of Catalytic Process (McGraw-Hill, New York, 1979) ch. 5.
- [2] R.J.H. Voorhoeve and J.C.M. Stuiver, J. Catal. 23 (1971) 228.
- [3] A.L. Farragher and P. Cossee, in: Proc. 5th Int. Congress on Catalysis, ed. J.W. Hightower (North Holland, Amsterdam, 1973) p. 1301.
- [4] H. Topsøe, B.S. Clausen, R. Candia, C. Wivel and S. Morup, J. Catal. 68 (1981) 433.
- [5] R.R. Chianelli and G. Berhault, Catal. Today 53 (1999) 357.
- [6] R.R. Chianelli and T.A. Pecoraro, US Patent 4 288 422 (1981).
- [7] R.R. Chianelli and T.A. Pecoraro, US Patent 4 826 797 (1989).
- [8] R.L. Seiver and R.R. Chianelli, US Patent 4 544 481 (1985).
- [9] G. Alonso, V. Petranovskii, M. Del Valle, J. Cruz-Reyes, A. Licea-Claverie and S. Fuentes, Appl. Catal. A 197 (2000) 87.
- [10] G. Alonso, M. Del Valle, J. Cruz-Reyes, V. Petranovskii, A. Licea-Claverie and S. Fuentes, Catal. Today 43 (1998) 117.
- [11] G. Berhault, A. Mehta, A.C. Pavel, J. Yang, L. Rendon, M.J. Yácaman, L. Cota Araiza, A. Duarte Moller and R.R. Chianelli, J. Catal. 198 (2001) 9.
- [12] H. Hallie, Oil Gas J. 80(48) (1982) 69.
- [13] R. Prada Silvy, P. Grange, F. Delannay and B. Delmon, Appl. Catal. 46 (1989) 113.
- [14] J. van Gestel, J. Leglise and J.-C. Duchet, J. Catal. 145 (1994) 429.
- [15] B. Dhandapani, T. St. Clair and S.T. Oyama, Appl. Catal. A 168

(1998) 219.

[16] V. Schwartz, V. Teixeira da Silva and S.T. Oyama, *J. Mol. Catal. A* 163 (2000) 87.

[17] C.H. Chang and S.S. Chan, *J. Catal.* 72 (1981) 139.

[18] E.Z. Diemann, *Z. Anorg. Allg. Chem.* 432 (1977) 127.

[19] G.L. Schrader and C.P. Cheng, *J. Catal.* 85 (1984) 488.

[20] K.S. Liang, R.R. Chianelli, F.Z. Chien and S.C. Moss, *J. Non-Cryst. Solids* 79 (1985) 251.

[21] R.R. Chianelli, *Int. Rev. Phys. Chem.* 2 (1982) 127.

[22] H.P. Wang, P. Skeldon, G.E. Thompson and G.C. Wood, *J. Mater. Sci.* 32 (1997) 497.

[23] M. Daage and R.R. Chianelli, *J. Catal.* 149 (1994) 414.

[24] R.R. Chianelli, *Catal. Rev. Sci. Eng.* 26 (1984) 361.

[25] D. Letourneur, R. Bacaud, M. Vrinat, D. Schweich and I. Pitault, *Ind. Eng. Chem. Res.* 37 (1998) 2662.

[26] V.B. Krebs and G. Gattow, *Z. Anorg. Allg. Chem.* 338 (1963) 225.

[27] J.P. Perchard, M.T. Forel and M.L. Josien, *J. Chim. Phys.* 61 (1964) 645.

[28] M. Ziolek, O. Saur, J. Lamotte and J.-C. Lavalley, *J. Chem. Soc. Faraday Trans.* 90 (1994) 1029.

[29] M.M. Disko, C.C. Ahn and B. Fultz, *Transmission Electron Energy Loss Spectrometry in Materials Science* (Booknews Inc., Portland, OR, 1992).

- [30] C. Glasson, Ph.D. thesis, University of Lyon, Lyon, France.
- [31] G. Alonso, M. Del Valle, J. Cruz, A. Licea-Claverie, V. Petranovskii and S. Fuentes, *Catal. Lett.* 52 (1998) 55.
- [32] P. Raybaud, J. Hafner, G. Kresse and H. Toulhoat, *Surf. Sci.* 407 (1998) 237.
- [33] J.S. Lee, L. Volpe, F.H. Ribeiro and M. Boudart, *J. Catal.* 112 (1988) 44.
- [34] B. Frühberger and J.G. Chen, *J. Am. Chem. Soc.* 118 (1996) 11599.
- [35] P. Raybaud, J. Hafner, G. Kresse and H. Toulhoat, *J. Phys.: Condens. Matter.* 9 (1997) 11107.
- [36] P.A. Aegerter, W.W.C. Quigley, G.J. Simpson, D.D. Ziegler, J.W. Logan, K.R. McCrea, S. Glazier and M.E. Bussell, *J. Catal.* 164 (1996) 109.
- [37] R.R. Chianelli, G. Berhault, P. Santiago, D. Mendoza, A. Espinosa, J.A. Ascensio and M.J. Yácaman, *Mat. Tech. Adv. Perf. Mat.* 15 (2000) 54.
- [38] C.B. Roxlo, H.W. Deckmann, J.H. Dunsmuir, A.F. Ruppert and R.R. Chianelli, *Mater. Res. Soc. Symp. Proc.* 82 (1987) 481.
- [39] R.R. Chianelli, A.F. Ruppert, S.K. Behal, B.H. Kear, A. Wold and R. Kershaw, *J. Catal.* 92 (1985) 56.
- [40] G. Berhault, M. Lacroix, M. Breysse, F. Maugé, J.-C. Lavalley, H. Nie and L. Qu, *J. Catal.* 178 (1998) 555.
- [41] M. Breysse, G. Berhault, S. Kasztelan, M. Lacroix, F. Maugé and G.

Pérot, Catal. Today 66 (2001) 15.

[42] J.S. Choi, G. Bugli and G. Djéga-Mariadassou, J. Catal. 193 (2000) 238.

[43] P.J. Mangnus, A. Riezebos, A.D. van Langeveld and J.A. Moulijn, J. Catal. 151 (1995) 178.

[44] G. Berhault, M. Lacroix, M. Breysse, F. Maugé, J.-C. Lavalley and L. Qu, J. Catal. 170 (1997) 37.

[45] J. Polz, H. Zeilinger, B. Müller and H. Knözinger, J. Catal. 120 (1989) 22.

[46] S.I. Kim and S.I. Woo, Appl. Catal. 74 (1991) 109.

[47] J.C. Duchet, E.M. van Oers, V.H.J. de Beer and R. Prins, J. Catal. 80 (1983) 386.